Electrocatalytic Properties of Pt Nanowires Supported on Pt and W Gauzes

Eric P. Lee,[†,⊥] Zhenmeng Peng,[‡,⊥] Wei Chen,[§] Shaowei Chen,[§] Hong Yang,[‡] and Younan Xia[†,*]

[†]Department of Biomedical Engineering, Washington University, St. Louis, Missouri 63130, [‡]Department of Chemical Engineering, University of Rochester, Rochester, New York 14627, and [§]Department of Chemistry and Biochemistry, University of California, Santa Cruz, California 95064. [⊥]These two authors contributed equally to this work.

ABSTRACT This paper describes the preparation of Pt- or W-supported Pt nanowires by directly growing them on the surface of Pt or W gauze. The growth direction of the nanowires was determined to be along the <111> axis. Electrochemical measurements were performed to investigate their catalytic performance toward methanol oxidation. It was found from cyclic voltammetry that the Pt nanowires supported on Pt gauze had the largest electrochemically active surface area with the greatest activity toward methanol oxidation reaction. They also exhibited a slightly slower current decay over time, indicating a higher tolerance to CO-like intermediates. Furthermore, electrochemical impedance spectroscopy measurements showed that the catalytic performance of the supported Pt nanowires prepared with a H_2PtCl_6 precursor concentration of 40 mM is significantly better for methanol oxidation than the samples prepared at a concentration of 80 mM. This was due partially to the incomplete removal of poly(vinyl pyrrolidone) (PVP) from the more concentrated sample. In contrast, the Pt nanowires supported on W gauze performed the worst.

KEYWORDS: platinum nanowires · platinum and tungsten support · high surface area · electrochemistry · methanol oxidation reaction

There is currently a great interest in developing different kinds of green technologies to power portable devices such as cell phones, computers, and cam recorders. With the constant rise in gas prices, the search for alternate fuels has also triggered an unrelenting search for sustainable energy. Whether the goal is to develop a cleaner source of energy, or simply just an alternate to petroleum, fuel cells have emerged as one of the most promising candidates. To this end, precious metals have continually proven to be the elite materials for fuel cell applications. Most notably, Pt and its alloys have been most widely used as the catalysts because of their excellent properties in the adsorption and dissociation of hydrogen, oxygen, and various other molecules.[1] Direct methanol fuel cell (DMFC) has recently attracted much attention and has been identified as a promising candidate to compete with conventional batteries for powering portable electronic devices.[2] For the standard DMFC device, Pt-based catalysts are employed as the anode because of their excellent performance in catalyzing the dehydrogenation of methanol, a key step in the direct oxidation of methanol to CO_2.[3] The active surface area of the catalyst can be greatly increased by reducing the size of the Pt nanoparticles and therefore creating a larger number of catalytically active centers for methanol oxidation reaction (MOR).[4] The efficiency of MOR can also be improved by changing the morphology of the Pt nanostructures from nanoparticle to nanowire, whose large side surface can provide additional catalytic active facets.[5]

The selection of a support for the Pt nanostructures is of critical importance to both the catalytic activity and durability.[6] In a conventional system, Pt is deposited on a conductive substrate such as carbon black or carbon nanotubes.[7,8] This system is intrinsically limited in terms of life span, and the catalytic surface area of the electrode may decrease with time.[6] To avoid the drawback of using carbon as a conductive support, we have demonstrated that Pt gauzes can just as easily be used as a conductive support to alleviate the issue of corrosion. Furthermore, the Pt support can contribute to enhancing the catalytic activity. Another issue that can potentially be solved by using functional supports is the poisoning by CO-like intermediates. It is well-documented that the Pt nanostructures are vulnerable to poisoning from CO-like intermediates formed during the oxidation of methanol and may become catalytically inactive over time.[9] To improve the CO tolerance of Pt-based catalysts, various techniques have been developed, among which utilization of W as a cocatalyst has been shown with great

*Address correspondence to xia@biomed.wustl.edu.

Received for review July 21, 2008 and accepted September 14, 2008.

Published online September 26, 2008.
10.1021/nn800458p CCC: $40.75

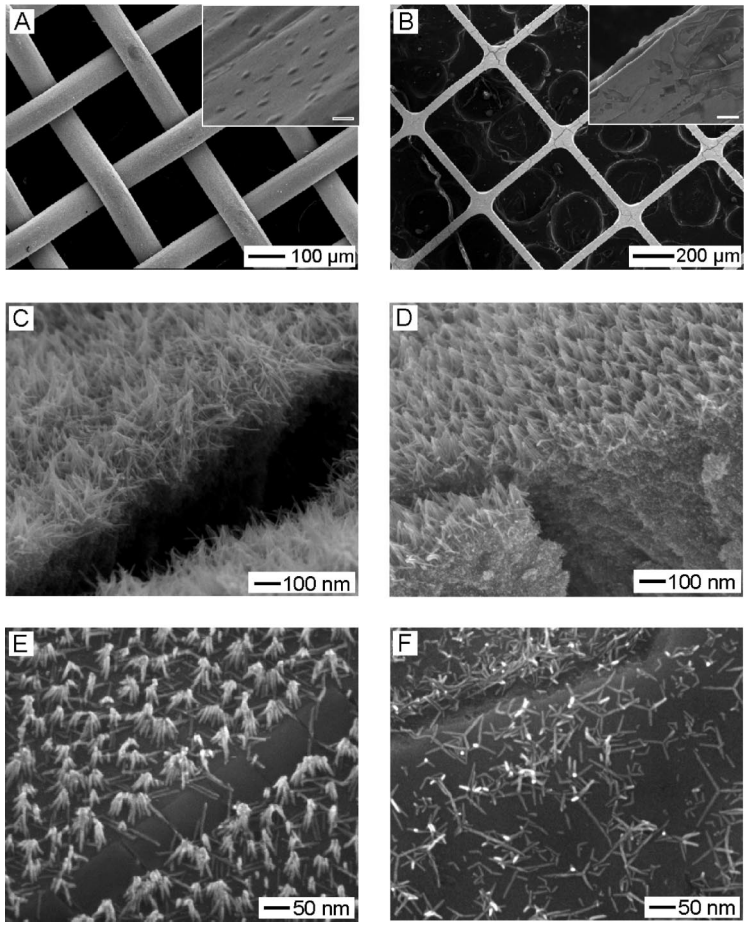

Figure 1. SEM images of (A) Pt and (B) W gauzes prior to Pt nanowire growth, with insets showing the detailed surface morphology. The scale bars in the insets are 200 nm. (C, D) SEM images of Pt nanowires on Pt and W gauzes, respectively, obtained as the final products of an iron-mediated polyol process by using a 1 mL solution of H_2PtCl_6 (80 mM). (E, F) SEM images of Pt nanowires grown on the surface of Pt and W gauzes, respectively, with the concentration of H_2PtCl_6 being reduced to 40 mM.

promise.[10] For this reason, we also used W gauzes as supports to take advantage of the cocatalytic effect of W on the oxidation of CO during MOR.

RESULTS AND DISCUSSION

Synthesis and Characterization of Pt Nanowires on Pt and W Gauzes. Figure 1 shows SEM images of typical samples before and after growing Pt nanowires on Pt and W gauzes. It is proposed that the highly irregular and rough surfaces (insets of Figure 1A,B) of the Pt and W gauzes serve as primary nucleation sites for the growth of Pt nanowires due to the higher surface energies associated with irregularities such as indentions, step edges, or protrusions, which significantly lower the barrier for nucleation.[11,12] A dense array of Pt nanowires could be directly grown on the surfaces of both Pt and W gauzes (Figure 1A,B, respectively) by following the iron-mediated polyol process, in which ethylene glycol (EG) serves as both a reducing agent and a solvent.[13] In this synthesis, Pt(II) species were formed by reducing H_2PtCl_6 with EG at 110 °C in the presence of poly(vinyl pyrrolidone) (PVP), which serves as a stabilizer. By adding 20 mM of $FeCl_3$ or $FeCl_2$, the Pt(II) species were reduced at an extremely slow rate, resulting in a kinetically controlled process that directs the growth of Pt atoms into uniform nanowires.

The samples in Figure 1C,D were prepared by injecting 1 mL of H_2PtCl_6 (80 mM) after preheating an EG solution for 1 h at 110 °C. In these cases, regardless of the gauze type, a supersaturation of Pt atoms, resulting from the reduction of the Pt(II) species, initially caused the nucleation and growth of Pt nanoparticles at the surface of the Pt or W gauze, which further evolved into agglomerates and larger structures until the concentration of Pt atoms fell to a critical level. At this point, the growth mechanism of the Pt atoms switched to a highly anisotropic mode to form uniform Pt nanowires. In order to bypass the nucleation of Pt nanoparticles and to utilize the Pt most efficiently for nanowire growth, the concentration of H_2PtCl_6 was reduced by one-half to 40 mM, resulting in the nucleation and growth of Pt atoms into nanowires directly on the surfaces of the Pt and W gauzes. Figure 1E,F shows SEM images of the samples verifying that the Pt nanowires indeed grew from the Pt and W gauzes without a layer of aggregated Pt nanoparticles. By lowering the concentration of H_2PtCl_6, the concentration of Pt atoms fell below the critical level at an earlier stage, thereby promoting the highly anisotropic growth and formation of Pt nanowires.

To assess the quality of the Pt nanowires and confirm that their growth direction is in fact along the <111> axis, high-resolution TEM images of single Pt nanowires released from the surface of Pt or W metal gauze were obtained (Figure 2). The Pt nanowires were prepared from 1 mL solution of 40 mM H_2PtCl_6. The fringe spacing of 0.23 nm corresponds to the interplanar separation between the {111} planes, indicating that the growth direction of the nanowires is along the <111> axis. This mechanism for the growth of Pt <111> nanowires on Pt agglomerates has been explored by our group in previous studies.[14] Both samples (Figure 2A,B) showed the same crystallographic characteristics indicating that the crystal growth of Pt nanowires is not affected by the substrate from which they grow.

Electrochemical Measurements. The electrochemically active surface area (ECSA) was studied based on hydrogen adsorption using cyclic voltammetry (CV). Note that the samples had only been washed by chloroform, ethanol, and distilled water and without any heat treatment, typically required for carbon-supported Pt catalysts. Figure 3 shows CV curves of four different samples in 0.5 M H_2SO_4 at a scan rate of 50 mV/s. It was found that Pt nanowires prepared on Pt gauze with a 1 mL solution of 40 mM H_2PtCl_6 had an active surface area that was almost four times greater than the pristine gauzes. For the case of Pt gauze (Figure 3A), the ECSA increased from 0.762 cm^2 for the pristine gauze to 3.01

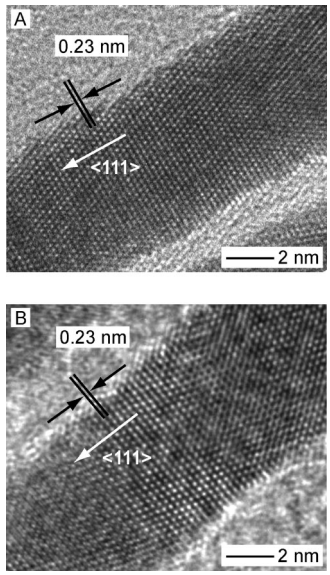

Figure 2. HRTEM images of individual Pt nanowires recorded along [011], prepared with a 1 mL solution of H_2PtCl_6 (40 mM), which were released from (A) Pt and (B) W gauze supports, respectively, *via* sonication. The fringe spacing of 0.23 nm corresponds to the interplanar separation between the {111} planes, implying that the growth direction of the nanowire is along the <111> axis.

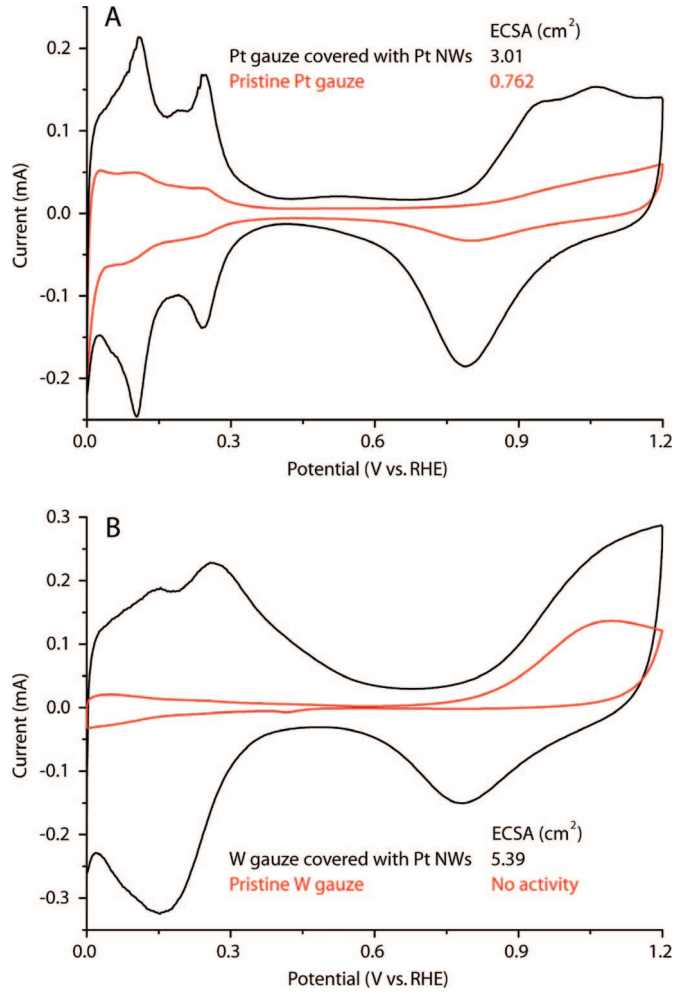

Figure 3. CV curves of pristine metal gauzes and metal gauzes covered with Pt nanowires grown from a 1 mL solution of H_2PtCl_6 (40 mM). The CVs were recorded in Ar-protected 0.5 M H_2SO_4 with a 50 mV/s scan rate. (A) Pristine Pt gauze and a Pt gauze covered by Pt nanowires, (B) a pristine W gauze and a W gauze covered by Pt nanowires. For all samples, the ECSA values were calculated from the backward potential curve (0.05 to 0.4 V *vs* RHE).

cm^2 for the nanowire-coated sample. The H adsorption/desorption features at ~0.12 V (*vs* RHE) are similar to what is observed for Pt(110) crystal faces reported in literature.[15−17] The more positive H adsorption peaks at ~0.23 V (*vs* RHE) can be attributed to the Pt(100) facets.[15−17] Since the H adsorption/desorption region observed for Pt(111) facets is essentially featureless (no peaks at potentials <0.12 V *vs* RHE), this suggests that there is a low presence of (111) facets.[17]

For the case of the pristine W gauze (Figure 3B), the ECSA for the adsorption/desorption of hydrogen over pristine W gauze was not observed; there is no obvious adsorption of hydrogen on W.[10,18] However, for the W gauze prepared with Pt nanowires, H adsorption/desorption activity was observed, but with rather unusual peaks. Instead of two peaks at ~0.12 and ~0.23 V (*vs* RHE), representing the (110) and (100) facets of Pt, there is one distinct large peak at ~0.26 V (*vs* RHE). Nagel and co-workers studied a similar case on W-modified, sputter-deposited Pt electrodes and observed that the more cathodic hydrogen adsorption peak was suppressed by W, resulting in the evolution of a new peak at 0.26 V (*vs* RHE) in the anodic sweep and at 0.21 V (*vs* RHE) in the cathodic sweep. This response was determined to be due to the oxidation of W, which overlapped with the hydrogen adsorption peaks.[10] On the basis of their findings, the W gauze may be oxidized during the potential scan, and therefore, the calculated ECSA value of 5.39 cm^2 does not give the exact active surface area of the sample (as the oxidation/reduction of W also occurs in the range of hydrogen adsorption/desorption). As a result, even though it is clear that the Pt nanowires supported on W gauze display active surfaces, an exact active surface area of the sample based on hydrogen adsorption cannot be determined.

The electrocatalytic activity of the Pt nanowires supported on Pt gauze was further measured by CV and chronoamperometry and benchmarked against an E-TEK 20 wt % Pt/C catalyst. Figure 4A shows the CV curves of methanol oxidation under acidic conditions (0.5 M CH_3OH and 0.5 M H_2SO_4) catalyzed by two samples prepared on Pt and W gauze, a pristine Pt gauze sample, and an E-TEK catalyst. Voltage sweeps were scanned in the range of 0−1.2 V at a rate of 50 mV/s. The voltammetric features are consistent with literature reports and are typical of the oxidation of methanol.[19−21] The Pt nanowires supported on Pt and W gauzes were prepared with a 1 mL solution of H_2PtCl_6 (40 mM), which corresponds to the samples seen in Figure 1E,F, respectively. The methanol oxidation peaks for the Pt nanowires supported on Pt and W gauzes and

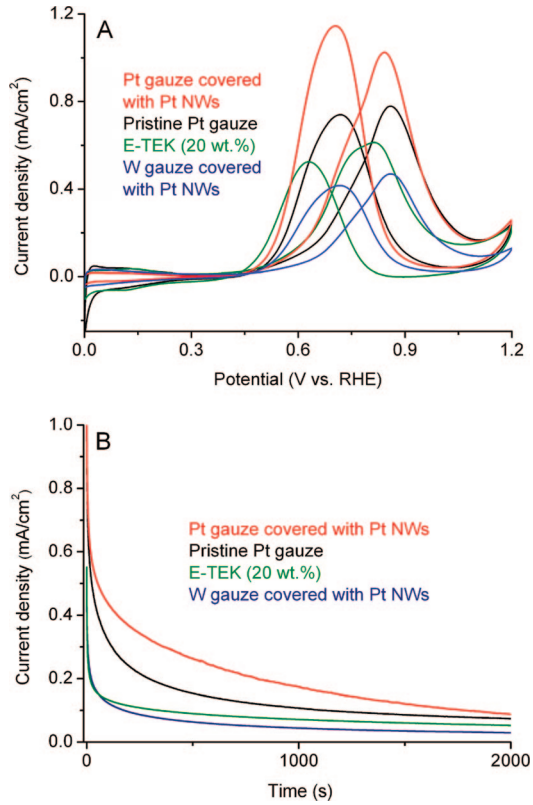

Figure 4. (A) CV curves for MOR in acidic solution. The Pt nanowires were prepared with a 1 mL solution of H_2PtCl_6 (40 mM) on Pt and W gauze. Electrolyte: 0.5 M H_2SO_4 + 0.5 M MeOH; scan rate = 50 mV/s. (B) Chronoamperometry curves at 0.85 V *vs* RHE in acidic solution. Electrolyte: 0.5 M H_2SO_4 + 0.5 M MeOH.

the pristine Pt gauze fully developed at 0.85 V (*vs* RHE) in the forward sweep and at 0.70 V in the backward sweep. The peak current densities associated with methanol oxidation in the forward scan were 1.02 mA/cm^2 for Pt nanowires supported on Pt gauze, 0.78 mA/cm^2 for pristine Pt gauze, and 0.47 mA/cm^2 for Pt nanowires supported on W gauze. However, it should be pointed out that the current density for Pt nanowires on W gauze is underestimated. As discussed earlier, the ECSA for Pt nanowires supported on W gauze (5.39 cm^2 from Figure 3B) is superficially determined from the adsorption/desorption of hydrogen and the oxidation/reduction of W. This results in an overestimation of the ECSA, and because the ECSA is used to normalize the area current density, 0.47 mA/cm^2 is an underestimated value. As a reference, the carbon-supported E-TEK 20 wt % Pt/C catalyst was tested, which had a peak current density of 0.61 mA/cm^2. The high activity of the Pt nanowires supported on Pt gauze, over 1.5 times the activity compared to that of E-TEK and over 1.3 times the activity compared to that of pristine Pt gauze, can be partially attributed to the different exposed facets of Pt. The rate of methanol oxidation has been found to be the highest on the Pt(110) facets among the low-index surfaces when using H_2SO_4 as the supporting electrolyte.[21−23] As indicated in Figure 3A, there are more exposed (110) facets on the Pt nanowires supported on Pt gauze as compared to the pristine Pt gauze (monitoring the peaks at ~0.12 V *vs* RHE), which will thereby lead to a higher activity.

Chronoamperometry data were recorded at 0.85 V (*vs* RHE) for 2000 s as a measure of the catalyst deactivation (Figure 4B). We observed that the Pt nanowires supported on Pt gauze exhibited a slower current decay over time in comparison to the pristine Pt gauze, indicating a larger catalytically active surface area and perhaps higher tolerance to CO-like intermediates. The enhancement may be partially attributed to a faster removal rate of the poisoning species on (110) facets of the Pt nanowires.[22] On the other hand, Pt nanowires supported on W gauze showed a faster current decay, indicating a negative effect of the W support for removal of the CO-like poisoning intermediates, which is contrary to what was observed by Nagel and coworkers.[10] After 2000 s of continuous operation, the current densities from the Pt nanowires supported on Pt gauze, pristine Pt gauze, E-TEK, and Pt nanowires supported on W gauze decayed to about 8.4, 9.4, 9.5, and 6.4%, respectively, of their initial values. These measurements indicate that all four samples exhibit comparatively similar responses to catalytic poisoning after extended continuous runs.

Electrochemical Impedance Spectroscopy Measurements. To further elaborate on the electron transfer kinetics of methanol oxidation on the Pt nanowire electrode, selected electrochemical impedance spectroscopy (EIS) measurements were then carried out. Figure 5 shows the representative Nyquist complex-plane impedance spectra of Pt nanowires supported on Pt gauze prepared with 1 mL of H_2PtCl_6 at concentrations of (A−C) 80 mM and (D−F) 40 mM (denoted with Pt-80 and Pt-40 nanowires, respectively) in 0.1 M CH_3OH and 0.1 M H_2SO_4 at varied electrode potentials from 0.00 to +1.20 V (shown as figure legends). At the Pt-80 electrode, the features are quite rich in the EIS study, as compared to the voltammetric profiles (Figure S1 in Supporting Information). At potentials more negative than +0.70 V (Figure 5A), the diameter of the impedance arcs increases with increasing electrode potential. This may be attributed to the increasing accumulation of CO on the surface of the Pt nanowires (as a result of the nonfaradaic dissociation of methanol), probably because of the incomplete removal of the PVP protecting layer that impedes the oxidative removal of surface-adsorbed CO. At more positive potentials, +0.75 to +0.85 V (Figure 5B), the impedance arcs start to appear in the second quadrant instead of the conventional first one. Such negative impedance behaviors have been observed in previous studies of the electrooxidation of methanol and formic acid on Pt and other Pt-based alloy electrodes and are ascribed to the oxidative removal of CO from the catalyst surface and the recovery of the catalytic active sites.[24−27] With a further

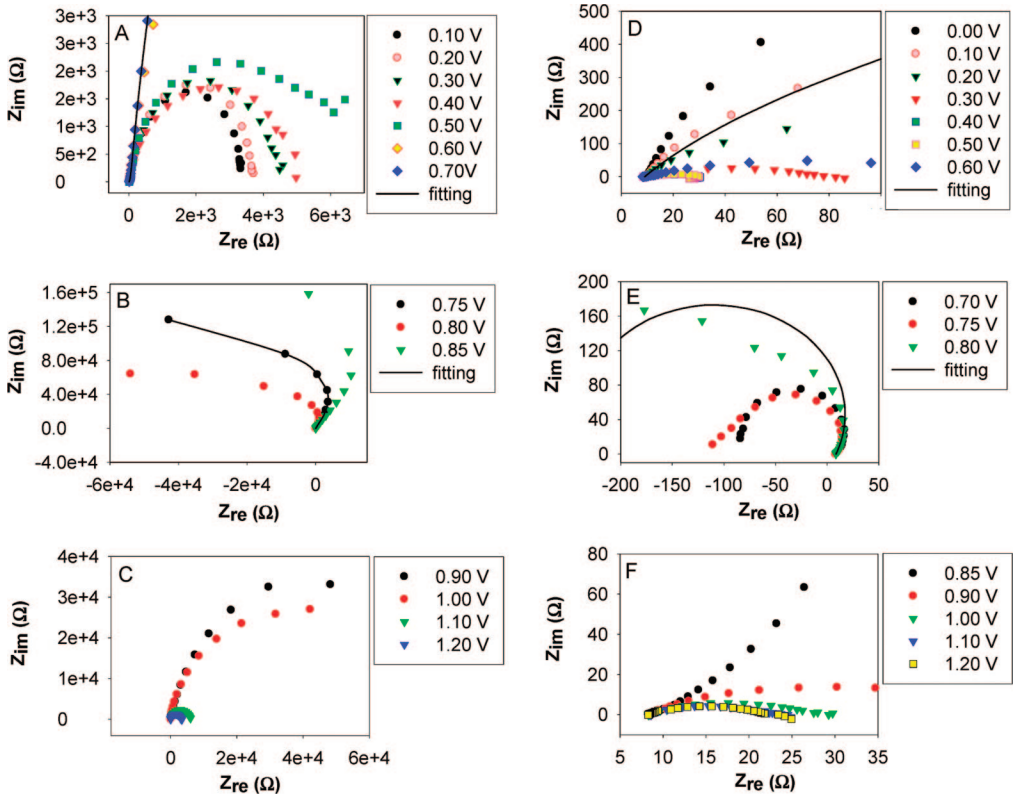

Figure 5. Complex-plane (Nyquist) impedance plots of the oxidation of methanol over Pt nanowires supported on Pt gauze prepared with 1 mL solutions of H_2PtCl_6 at concentrations of (A−C) 80 mM and (D−F) 40 mM in 0.1 M CH_3OH and 0.1 M H_2SO_4. The electrode potentials are shown as figure legends. Solid lines are representative simulations based on the equivalent circuits shown in Figure S2 in Supporting Information.

increase of the electrode potential, > +0.85 V (Figure 5C), the impedance changes from negative to normal positive and the diameter of the arcs decreases with increasing electrode potentials, indicating faster electron transfer kinetics at higher potentials. At these sufficiently positive potentials, CO adsorbed on the Pt surface was completely removed and the surface reaction sites occupied by CO were recovered, and hence the diminishment of charge transfer resistance.

The EIS behaviors are somewhat different at the Pt-40 electrode (Figure 5D−F). First, the diameter of the arcs decreases with increasing potential at potentials lower than +0.60 V (Figure 5D), suggesting more active sites are available for methanol oxidation. At potentials higher than +0.70 V (Figure 5E), negative impedance appears in the second quadrant and then returned to normal at +0.85 V (Figure 5F) with the diameter of the arcs decreasing with increasing electrode potential. Note that the onset potential of negative impedance (+0.70 V) is somewhat more negative than that with the Pt-80 electrode (+0.75 V), implying the oxidative removal of CO is facilitated at the Pt-40 electrode as compared to that at the Pt-80 electrode. From Figure 5, it can also be seen that the diameter of the impedance arcs at the Pt-40 electrode is significantly smaller than that at the Pt-80 electrode, indicating substantially lower charge transfer resistance for methanol oxidation; that is, the catalytic activity of Pt-40 nanowires is much higher than that of Pt-80 nanowires for methanol electro-oxidation, as suggested in the aforementioned voltammetric study.

Furthermore, from the fitting by the equivalent circuit (Figure S2 in Supporting Information), the variation of the charge transfer resistance (R_{CT}) with electrode potentials can be quantitatively evaluated (Figure S3 in Supporting Information). Overall, R_{CT} at the Pt-40 nanowires is about 3 orders of magnitude smaller than that at the Pt-80 nanowires, indicating the electron transfer kinetics for methanol oxidation at the Pt-40 electrode is much better facilitated.

The drastic difference in catalytic performance for methanol oxidation on Pt-80 and Pt-40 nanowires can be interpreted on the basis of the structure of the nanowire films. At least part of it may be ascribed to the incomplete removal of PVP from the Pt-80 electrode surface, which hinders the accessibility of the catalyst surface by the fuel molecules as well as oxidative removal of CO from the electrode surface. As a result, Pt nanowires prepared with an H_2PtCl_6 concentration of 40 mM on Pt and W gauze were used for electrochemical measurements to determine the catalytic activity of the samples toward the oxidation of methanol.

CONCLUSIONS

On the basis of methanol oxidation, the electrocatalytic activity increases in the sequence of Pt nanowires

supported on W gauze < pristine Pt gauze < Pt nanowires supported on Pt gauze. The high activity of the sample supported on Pt gauze can be explained in part by the greater exposure of Pt(110) facets associated with the Pt nanowires. From CV experiments performed in H_2SO_4, there is a large oxidation peak at ~0.12 V for the Pt nanowires supported on Pt gauze, indicating a large concentration of Pt(110) facets. While the Pt nanowires supported on W gauze indicated the largest ECSA, its activity toward MOR was the lowest. This is because the large ECSA value was determined to be an overestimation due to the signal overlap between the oxidation/reduction of W and the adsorption/desorption of hydrogen, and the lower activity toward MOR is expected as W does not have any catalytic contribution to the oxidation of methanol. It was also determined that increasing the density of Pt nanowires makes it difficult to completely remove PVP from the sample, which impedes the oxidative removal of surface-adsorbed CO and hinders the accessibility of the catalytic surface by the fuel molecules. According to EIS measurements, the catalytic performance of Pt-40 nanowires for methanol oxidation is significantly larger than that of the Pt-80 nanowires, due partially to the incomplete removal of PVP from the later sample. Chronoamperometry data indicated that all samples exhibited similar responses to catalytic poisoning after 2000 s of continuous operation. However, the Pt nanowires supported on Pt gauze exhibited a slightly slower current decay over time, indicating a higher tolerance to CO-like intermediates. The results described in the present work demonstrate a new type of conductive support, which can be used to grow dense arrays of Pt nanowires for use as active components in high-power density fuel cell applications.

EXPERIMENTAL SECTION

Synthesis of Pt- and W-Supported Pt Nanowires. In a typical procedure, 4 mL of EG (J.T. Baker, Lot# A34B16) was injected into a three-neck flask (fitted with a reflux condenser and a Teflon-coated stir bar) and heated in air to 110 °C for 30 min. A Pt gauze (5 mm × 5 mm, Alfa Aesar, 100 mesh woven from 0.0762 mm diameter wire, 99.9% metals basis) or W gauze (5 mm × 5 mm, Alfa Aesar, 100 mesh woven from 0.0254 mm diameter wire) was then added to the EG along with 20 μL of a 20 mM iron species ($FeCl_3 \bullet 6H_2O$ or $FeCl_2 \bullet 6H_2O$, Aldrich, predissolved in EG). The solution was heated for an additional 30 min to boil off any trace amount of water; 400 mM PVP (MW = 55 000, 0.045 g, Aldrich) and 80 mM H_2PtCl_6 (0.033 g, Aldrich) were dissolved separately in 2 mL of EG at room temperature. These two solutions, each of 1 mL in volume, were then added simultaneously into the flask over a period of 1.5 min. The molar ratio between H_2PtCl_6 and the repeating unit of PVP was 1:5. The reaction mixture was continued with heating at 110 °C in air. After the reaction had proceeded for 18 h, the final solution was colorless with black aggregates on the Pt gauze and at the bottom of the flask. The Pt gauze was washed thoroughly with ethanol and water to remove EG and excess PVP.

SEM and TEM Characterization. The SEM samples were prepared by placing the as-prepared silicon substrates on a carbon tape, washing with a large volume of water, and drying under ambient conditions. SEM images were taken using a Sirion XL field-emission microscope (FEI, Hillsboro, OR) operated at an acceleration voltage in the range of 10−15 kV. High-resolution TEM images were performed using a JEOL JEM-2100F microscope operated at an accelerating voltage of 200 kV.

Electrochemical Measurements. Prior to the electrochemical measurements, the Pt and W gauze samples were thoroughly washed with chloroform, ethanol, and finally distilled water. The electrochemical properties were examined with a CHI 760 dual channel electrochemical workstation (CH instruments, Inc.) using a three-electrode system, which consists of a working electrode made of 5 mm × 5 mm sample gauze connected by a Au wire, a Pt wire counter electrode, and an RHE reference electrode (Gaskatel, HydroFlex). Hydrogen adsorption−desorption CV data were recorded in an argon-protected 0.5 M sulfuric acid aqueous solution. This solution was purged with argon for 30 min first to deplete dissolved oxygen. After the purge, a continuous stream of argon was introduced into the cell above the liquid surface to maintain an inert atmosphere over the testing solution. The CV was recorded between 0.0 and 1.2 V *vs* RHE with a scan rate of 50 mV/s. The region for hydrogen adsorption (0.05 to 0.4 V *vs* RHE on the backward potential scan) was used to estimate the ECSA values.

For CVs and chronoamperometry of the MOR, an air-free aqueous solution containing 0.5 M CH_3OH and 0.5 M H_2SO_4 was used. The CV was recorded between 0.0 and 1.2 V *vs* RHE with a scan rate of 50 mV/s. Before recording chronoamperometry curves, the potential of the working electrode (samples) was cycled several times then preset at 0 V for 30 s to remove any contaminants or oxidants on the surface.

Electrochemical Impedance Spectroscopy (EIS) Measurements. EIS measurements were carried out using an EG&G PARC potentiostat/galvanostat model 283 and frequency response detector (model 1025). The impedance spectra were recorded between 100 kHz and 10 mHz with the amplitude (rms value) of the ac signal at 10 mV.

Acknowledgment. This work was supported in part by research grants from the NSF (DMR, 0451788 and 0804088) and ACS (PRF-44353-AC10).

Supporting Information Available: CV curves for MOR with Pt nanowires prepared on Pt gauze (Figure S1); equivalent circuits for the electro-oxidation of methanol (Figure S2); R_{CT} of methanol electro-oxidation at different electrode potentials on Pt nanowires supported on Pt gauze (Figure S3); complex-plane (Bode plots) impedance plots of the methanol oxidation on Pt nanowires supported on Pt gauze (Figure S4). This material is available free of charge *via* the Internet at http://pubs.acs.org.

REFERENCES AND NOTES

1. Teng, X. W.; Liang, X. Y.; Maksimuk, S.; Yang, H. Synthesis of Porous Platinum Nanoparticles. *Small* **2006**, *2*, 249–253.
2. Liang, Z. X.; Zhao, T. S. New DMFC Anode Structure Consisting of Platinum Nanowires Deposited into a Nafion Membrane. *J. Phys. Chem. C* **2007**, *111*, 8128–8134.
3. Liu, H. S.; Song, C. J.; Zhang, L.; Zhang, J. J.; Wang, H. J.; Wilkinson, D. P. A Review of Anode Catalysis in the Direct Methanol Fuel Cell. *J. Power Sources* **2006**, *155*, 95–110.
4. Hepel, M.; Dela, I.; Hepel, T.; Luo, J.; Zhong, C. J. Novel Dynamic Effects in Electrocatalysis of Methanol Oxidation on Supported Nanoporous TiO_2 Bimetallic Nanocatalysts. *Electrochim. Acta* **2007**, *52*, 5529–5547.
5. Lee, E. P.; Peng, Z.; Cate, D. M.; Yang, H.; Campbell, C. T.; Xia, Y. Growing Pt Nanowires as a Densely Packed Array on Metal Gauze. *J. Am. Chem. Soc.* **2007**, *129*, 10634–10635.
6. Yu, X. W.; Ye, S. Y. Recent Advances in Activity and Durability Enhancement of Pt/C Catalytic Cathode in PEMFC. *J. Power Sources* **2007**, *172*, 145–154.

7. Su, F.; Zeng, J.; Bao, X.; Yu, Y.; Lee, J. Y.; Zhao, X. S. Preparation and Characterization of Highly Ordered Graphitic Mesoporous Carbon as a Pt Catalyst Support for Direct Methanol Fuel Cells. *Chem. Mater.* **2005**, *17*, 3960–3967.
8. Zheng, S. F.; Hu, J. S.; Zhong, L. S.; Wan, L. J.; Song, W. G. *In Situ* One-Step Method for Preparing Carbon Nanotubes and Pt Composite Catalysts and Their Performance for Methanol Oxidation. *J. Phys. Chem. C* **2007**, *111*, 11174–11179.
9. Wee, J. H.; Lee, K. Y. Overview of the Development of CO-Tolerant Anode Electrocatalysts for Proton-Exchange Membrane Fuel Cells. *J. Power Sources* **2006**, *157*, 128–135.
10. Nagel, T.; Bogolowski, N.; Samjeske, G.; Baltruschat, H. On the Effect of Tungsten on CO Oxidation at Pt Electrodes. *J. Solid State Electrochem.* **2003**, *7*, 614–618.
11. Gouldstone, A.; Van Vliet, K. J.; Suresh, S. Nanoindentation: Simulation of Defect Nucleation in a Crystal. *Nature* **2001**, *411*, 656.
12. Brune, H. Microscopic View of Epitaxial Metal Growth: Nucleation and Aggregation. *Surf. Sci. Rep.* **1998**, *31*, 125–229.
13. Chen, J.; Herricks, T.; Geissler, M.; Xia, Y. Single-Crystal Nanowires of Platinum Can Be Synthesized by Controlling the Reaction Rate of a Polyol Process. *J. Am. Chem. Soc.* **2004**, *126*, 10854–10855.
14. Chen, J.; Xiong, Y.; Yin, Y.; Xia, Y. Surfactant-Directed Assembly of Pt Nanoparticles into Colloidal Spheres and Their Use as Substrates in Forming Pt Nanorods and Nanowires. *Small* **2006**, *2*, 1340–1343.
15. Yamamoto, K.; Kolb, D. M.; Kotz, R.; Lehmpfuhl, G. Hydrogen Adsorption and Oxide Formation on Platinum Single Crystal Electrodes. *J. Electroanal. Chem.* **1979**, *96*, 233–239.
16. Yeager, E.; O'Grady, W. E.; Woo, M. Y. C.; Hagans, P. Hydrogen Adsorption on Single Crystal Platinum. *J. Electrochem. Soc.* **1978**, *125*, 348–349.
17. Schmidt, T. J.; Fasteiger, H. A.; Stab, G. D.; Urban, P. M.; Kolb, D. M.; Behm, R. J. Characterization of High-Surface-Area Electrocatalysts Using a Rotating Disk Electrode Configuration. *J. Electrochem. Soc.* **1998**, *145*, 2354–2358.
18. Greeley, J.; Mavrikakis, M. Surface and Subsurface Hydrogen: Adsorption Properties on Transition Metals and Near-Surface Alloys. *J. Phys. Chem. B* **2005**, *109*, 3460–3471.
19. Esteban, P. O.; Leger, J. M.; Lamy, C.; Genies, E. Electrocatalytic Oxidation of Methanol on Platinum Dispersed in Polyaniline Conducting Polymers. *J. Appl. Electrochem.* **1989**, *19*, 462–464.
20. Wasmus, S.; Kuver, A. Methanol Oxidation and Direct Methanol Fuel Cells: A Selective Review. *J. Electroanal. Chem.* **1999**, *461*, 14–31.
21. Hamnett, A. Mechanism and Electocatalysis in the Direct Methanol Fuel Cell. *Catal. Today* **1997**, *38*, 445–457.
22. Kita, H.; Gao, Y.; Nakato, T.; Hattori, H. Effect of Hydrogen Sulphate Ion on the Hydrogen Ionization and Methanol Oxidation Reactions on Platinum Single-Crystal Electrodes. *J. Electroanal. Chem.* **1994**, *373*, 177–183.
23. Herrero, E.; Fanaszczuk, K.; Wiechowski, A. Electrochemistry of Methanol at Low Index Crystal Planes of Platinum: An Integrated Voltammetric and Chronoamperometric Study. *J. Phys. Chem.* **1994**, *98*, 5074–5083.
24. Hsing, I. M.; Wang, X.; Leng, Y. J. Electrochemical Impedance Studies of Methanol Electro-Oxidation on Pt/C Thin Film Electrode. *J. Electrochem. Soc.* **2002**, *149*, A615−A621.
25. Chen, W.; Kim, J.; Sun, S. H.; Chen, S. W. Electro-Oxidation of Formic Acid Catalyzed by FePt Nanoparticles. *Phys. Chem. Chem. Phys.* **2006**, *8*, 2779–2786.
26. Chen, W.; Kim, J. M.; Sun, S. H.; Chen, S. W. Composition Effects of FePt Alloy Nanoparticles on the Electro-Oxidation of Formic Acid. *Langmuir* **2007**, *23*, 11303–11310.
27. Chen, W.; Kim, J. M.; Xu, L. P.; Sun, S. H.; Chen, S. W. Langmuir−Blodgett Thin Films of $Fe_{20}Pt_{80}$ Nanoparticles for the Electrocatalytic Oxidation of Formic Acid. *J. Phys. Chem. C* **2007**, *111*, 13452–13459.